DNA damage-induced phosphorylation of histone H2A at serine 15 is linked to DNA end resection

Salar Ahmad, Valérie Côté and Jacques Côté#

St-Patrick Research Group in Basic Oncology, Centre Hospitalier Universitaire de Québec-Université Laval Research Center, Laval University Cancer Research Center, Quebec City, QC, G1R 3S3, Canada

Running Title: Phosphorylation of H2AS15 at DNA breaks

Corresponding authors: jacques.cote@crhdq.ulaval.ca

Word Count

Introduction, Results and Discussion: 3,138

Materials and Methods: 1,118

23 **ABSTRACT**

24 The repair of DNA double-strand breaks (DSBs) occurs in chromatin and several histone post-
25 translational modifications have been implicated in the process. Modifications of histone H2A
26 N-terminal tail has also been linked to DNA damage response, through acetylation or
27 ubiquitination of lysine residues that regulate repair pathway choice. Here, we characterize a
28 new DNA damage-induced phosphorylation on chromatin, at serine 15 of H2A in yeast. We
29 show that this SQ motif functions independently of the classical S129 C-terminal site (γH2A) and
30 mutant mimicking constitutive phosphorylation increases cell sensitivity to DNA damage.
31 H2AS129ph is induced by Tel1^{ATM} and Mec1^{ATR}, and loss of Lcd1^{ATRIP} or Mec1 signaling
32 decreases γH2A spreading distal to the DSB. In contrast, H2AS15ph is completely dependent on
33 Lcd1^{ATRIP}, indicating that this modification only happens when end resection is engaged. This is
34 supported by an increase of RPA and a decrease in DNA signal near the DSB in the *H2AS-15E*
35 phosphomimic mutant, indicating higher resection. This serine is replaced by a lysine in
36 mammals (H2AK15), which undergoes an acetyl-monoubiquityl switch to regulate binding of
37 53BP1 and resection. This regulation seems functionally conserved with budding yeast H2AS15
38 and 53BP1-homolog Rad9, using different post-translational modifications between organisms
39 but achieving the same function.

40

41

42

43 **INTRODUCTION**

44 The genetic information of the cell is challenged by various endogenous and exogenous cues
45 which leads to DNA damage. If unchecked, this can lead to mutations, translocations, loss of
46 genetic information and, in higher eukaryotes, be the underlying cause for diseases such as
47 cancer (1, 2). One of the most harmful form of DNA damage is DNA double-strand break (DSB).
48 To endure and mitigate such damage to the DNA, cells orchestrate cell cycle arrest and DNA
49 repair pathways, collectively termed the DNA damage response (DDR). Two main pathways to
50 repair DSBs are non-homologous end joining (NHEJ) and homologous recombination (HR). NHEJ
51 involves direct ligation of the two broken DNA ends which may require some processing,
52 making it a more error-prone pathway (3). In HR, single-stranded DNA (ssDNA) is generated
53 through a process called resection and involves the use of homologous sequence or sister
54 chromatid as a template to copy the genetic information, ensuring a lower error rate (4).

55 The phosphatidylinositol-3-OH kinase-related kinases (PIKKs) family plays an important
56 role in DDR. It includes *S. cerevisiae* Tel1 and Mec1 and mammalian ataxia telangiectasia-
57 mutated (ATM), AT-related (ATR) and DNA-dependent protein kinase (DNA-PK) (5, 6). One of
58 the first DNA damage-dependent chromatin modification to be identified was γ-H2A(X), which
59 is the phosphorylation of histone H2A at S129 in yeast and H2A.X at S139 in mammals (7-9).
60 This phosphorylation is carried out by both Tel1/ATM and Mec1/ATR. In yeast, H2AS129ph
61 spreads more than 50Kb on both sides flanking the DSB, whereas in mammals it covers up to a
62 megabase (10, 11). This histone mark is implicated in the DNA damage response and is required
63 for proper recruitment of several repair/signaling factors as well as chromatin
64 remodelers/modifiers (12-17). $H2AX^{-/-}$ mice are radiation sensitive, growth retarded, immune

65 deficient and show recruitment defect for a variety of repair factors such as Nbs1, 53BP1 and
66 BRCA1 (18).

67 Interestingly, budding yeast has another Tel1/Mec1-dependent SQ phosphorylation site
68 at H2B C-terminus, H2BT129ph, which largely correlates with H2AS129ph but is modulated by it
69 (10). Other DNA damage-induced phosphorylation marks have been mapped on chromatin but
70 are not deposited by PIKKs. These include H4S1ph, H2AS122ph and H2AT126ph in yeast, which
71 have been linked to processes like chromatin restoration after repair, meiosis, HR and repair of
72 fragile sites with CAG/CTG repeats (19-23). Apart from phosphorylation, other histone
73 modifications like acetylation, methylation, ubiquitylation and SUMOylation have been
74 implicated in DDR (16). In mammals H2AK15 is ubiquitinated by RNF168 and this mark is
75 responsible for recruitment and repair foci formation of 53BP1 in combination with H4K20me2,
76 inhibiting resection and favoring NHEJ (24). At DSBs, the TIP60 complex can acetylate H2AK15
77 and binds H4K20me, thus antagonizing 53BP1 and favoring repair by HR (25). In budding yeast,
78 Rad9 is the functional homolog of 53BP1, contains a Tudor domain which binds H3K79me
79 (equivalent to mammalian H4K20) and a BRCT domain which recognizes γ-H2A (17, 26, 27).
80 Both domains are required for the recruitment and retention of Rad9 at DSBs (17, 28). In
81 contrast to 53BP1, Rad9 does not have a ubiquitin-binding domain neither the yeast H2A has
82 lysine corresponding to human H2AK15 (**Fig. 1A**). Instead, yeast H2A has a SQ site at this
83 position which has been found phosphorylated in a Mec1-dependent manner upon DNA
84 damage, in a large phosphoproteomic study (29).

85 This led us to investigate whether H2AS15 had a role in the repair of DNA breaks. Our
86 results indicate that H2AS15ph is induced by $Mec1^{ATR}$ over a large domain of chromatin around

87 the DSB. We also present data arguing that H2AS15ph regulates Rad9 binding and DNA end
88 resection. Altogether, these results suggest an evolutionary conserved mechanism, similar to
89 the mammalian H2AK15 ubiquitin/acetylation switch, modulating yeast Rad9^{53BP1} function on
90 the chromatin surrounding DNA breaks.
91
92 **RESULTS**
93 **H2AS15ph function is distinct from H2AS129ph in response to DNA damage**
94 In order to investigate if H2A-S15 has a role in DNA damage response, we mutated H2A-S15 to
95 alanine (non-phosphorylation mimicking) or glutamic acid (phosphorylation mimicking). In the
96 presence of DNA damaging agent methyl methanesulfonate (MMS), *H2A-S15E* mutant cells
97 show a slight growth defect, which is not seen for *H2A-S15A* (**Fig. 1B**). However, in combination
98 with the *H2A-S129A* mutant, both *H2A-S15A/E* show stronger growth defect compared to single
99 *H2A-S129A* mutant cells (**Fig. 1B**). Next, we tested if the *H2A-S15* mutants had any genetic
100 interaction with the other PIKK-dependent histone phosphorylation induced in response to
101 DSBs in yeast, H2BT129ph (10). *H2A-S15A/E H2B-T129A* double mutant cells do not show any
102 additional growth defect compared to *H2A-S15* single mutants in presence of MMS (**Fig. 1C**).
103 These results indicate that H2AS129 and H2AS15 phosphorylations play distinct roles in
104 response to DNA damage induced by MMS.
105 To decipher if the *H2A-S15* mutants affect H2AS129 phosphorylation *in vivo*, we
106 performed ChIP-qPCR at an inducible DSB. We used the yeast background in which a single
107 persistent DNA double strand break is created at the *MAT* locus by the homothallic
108 endonuclease (HO), inducible by galactose-containing media. The induced H2AS129ph signal

109 detected on each side of the DSB in wild type (WT) cells corresponds to what was previously
110 reported (10, 12). Both *H2A-S15A/E* mutants show similar pattern of H2AS129ph compared to
111 WT cells, not affecting the induction or spreading of H2A-S129ph beside a very small increase in
112 the *H2A-S15E* mutant (**Fig. 1D-E**). These results again support a role of H2AS15ph in DNA
113 damage response/repair that is distinct from H2AS129ph.

114 The lysine residues of H2A and H4 N-terminal tails are known targets of the NuA4
115 acetyltransferase complex (30). Studies have described histone modifications modulating the
116 occurrence of other modifications in chromatin, thus forming a network of histone crosstalk
117 (16). H4S1ph carried out by CK2 has been shown to inhibit acetylation of various lysine residues
118 on the N-terminal tail of H4 and play an active role in DSB repair as well as transcription (19,
119 20). This raised the question whether H2AS15ph could influence acetylation of lysine residues
120 on the H2A and H4 N-terminal tails. Western blot analysis of whole cell extracts from yeast
121 cells harboring the *H2A-S15* point mutants and grown in normal conditions reveals a small
122 decrease in both H2A and H4 acetylation, more noticeable for the *H2A-S15A* mutant compared
123 to wild type (**Fig. 1F**). We further investigated *in vivo* if the *H2A-S15* mutants affected the
124 acetylation of histones around DSBs. Both *H2A-S15A/E* mutants show a decrease in H4
125 acetylation signal but only close to the DNA break site (**Fig. 1G**). These results suggest that
126 H2AS15ph has a small but significant effect on other histone modifications in regions
127 surrounding the DSB.

128

129 **H2AS15ph is induced over a large chromatin domain surrounding DNA double-strand breaks**

130 To characterize the dynamics of H2AS15ph in response to DNA damage, we produced and
131 purified an antibody against the *S. cerevisiae* H2A N-terminal portion with Ser15 bearing the
132 phosphorylation mark. To demonstrate that H2AS15ph is indeed regulated by DNA damage, we
133 performed immunoblotting with purified yeast native chromatin. As shown in **figure 2A**,
134 H2AS15ph signal increases with MMS treatment, similarly to H2AS129ph. A control using
135 phosphatase treatment of the chromatin confirms that the signal detected by the antibody is
136 indeed phosphorylation-specific (**Fig. 2B**).

137 To determine whether H2AS15ph occurs at the DSB, we performed ChIP-qPCR at the
138 *MAT* locus before and after HO induction. The signal detected for H2AS15ph shows a clear
139 increase around the DSB site in WT background spanning over 10 kilobases on each side of the
140 break (**Fig. 2C**). As a control to check the specificity of the signal detected by the antibody, the
141 *H2A-S15A* mutant cells do not show such signal over a large domain after induction of the DSB
142 (**Fig. 2C**). However, close to the break site, *H2A-S15A* mutant cells do show a slight increase
143 which likely reflects some non-specific cross-reactivity of the antibody with another mark. To
144 characterize the dynamics of H2AS15ph appearance around the DSB, the ChIP-qPCRs were
145 performed at different time-points after induction of the HO endonuclease. Interestingly,
146 appearance of H2AS15ph seems delayed in comparison to H2AS129ph, reaching maximum
147 levels throughout the region after 3hrs, while H2AS129ph reaches its maximum levels at 3 and
148 7kb within an hour (**Fig. 2D-E**). Since H2AS129ph seems deposited before H2AS15ph, we tested
149 if it is required for H2AS15 phosphorylation to occur. ChIP-qPCR in wild type and H2AS129A
150 mutant cells does show a significant decrease of H2AS15ph signal around the HO-induced DSB,
151 but the mark is still present (**Fig. 2F**). These results indicate that γH2A/H2AS129ph can influence

152 phosphorylation of H2AS15 around the DSB but is not *per se* required for it to occur, in
153 agreement with the increase DNA damage sensitivity of the double mutants (**Fig. 1B**).
154 Altogether, these data clearly demonstrate that H2AS15ph is actively deposited over a large
155 region of chromatin surrounding DNA double-strand breaks.
156

157 **Mec1^{ATR} is solely responsible for H2AS15 phosphorylation at DSBs**

158 Tel1^{ATM} and Mec1^{ATR} signaling kinases phosphorylate histone H2AS129 to form γ-H2A (7, 11,
159 31). They also target various proteins to modulate DSB repair and checkpoint activation.
160 Recruitment of Tel1 to DSB requires Xrs2 (mammalian NBS1), subunit of the Mre11-Rad50-Xrs2
161 (MRX) complex (32). Deletion of *XRS2* affects Tel1-dependent checkpoint signaling and
162 telomere maintenance functions (33). Yeast Lcd1/Ddc2 (mammalian ATRIP) is responsible for
163 the recruitment of Mec1 to RPA-coated single-stranded DNA (ssDNA) produced during end
164 resection (34). Mec1 has been shown to be involved in spreading of γ-H2A in *trans* onto
165 adjacent undamaged chromosomes in close physical proximity (10, 35). Deletion of *LCD1* leads
166 to loss of Mec1 recruitment to RPA-coated ssDNA and, therefore, Mec1-dependent cell
167 signaling in response to damage (36, 37).

168 *lcd1*Δ and *lcd1*Δ*xrs2*Δ mutant cells are respectively defective in the recruitment of Mec1
169 and both Mec1/Tel1 at the DSB. In *lcd1*Δ cells, where Tel1 recruitment and signaling is
170 unaffected, ChIP-qPCR experiments show that the signal for γ-H2A close to the break is similar
171 to wild type cells (**Fig. 3A**). However, farther from the break, at 7Kb and 10Kb, the signal is
172 significantly reduced, showing its relation to Mec1. In *lcd1*Δ*xrs2*Δ cells, where both Mec1 and
173 Tel1 recruitments are abrogated, the γ-H2A signal is completely abolished throughout the

174 region (**Fig. 3A**). This is similar to what has been observed for *mec1*Δ and *mec1*Δ*tel1*Δ mutant
175 cells in previous studies (10). Loss of *MEC1* affects γ-H2A spreading away from the break site,
176 whereas loss of *MEC1* and *TEL1* results in complete loss of γ-H2A.

177 A large scale phosphoproteomic study has detected phosphorylation of H2AS15 and
178 linked it to Mec1 (29). To investigate this, we carried out ChIP-qPCR using the H2AS15ph
179 antibody to study its spreading around the DSB in *lcd1*Δ and *lcd1*Δ*xrs2*Δ mutant cells. As shown
180 above, wild type cells show enrichment for H2AS15ph over a large region on each side of the
181 DSB (**Fig. 3B**). However, *lcd1*Δ as well as *lcd1*Δ*xrs2*Δ mutant cells do not show any H2AS15ph
182 signal. These results demonstrate that, unlike γ-H2A which is deposited by both the Mec1 and
183 Tel1 kinases, H2AS15 phosphorylation is carried out solely by Mec1, which links it to DNA end
184 resection after DSB formation.

185

186 **H2AS15 is required to maintain fidelity of resection**

187 Previous studies have shown that the *H2A-S129A* non-phosphorylation mutant leads to faster
188 resection from the HO-induced DSB compared to wild type cells (38, 39). This increased
189 resection may be attributed to the inability of Rad9 to bind H2AS129ph through its BRCT
190 domain, an essential interaction for its recruitment on chromatin (17, 27, 28, 40, 41). Budding
191 yeast Rad9, like its mammalian homolog 53BP1, functions in slowing down or keeping a check
192 on the rate of DNA end resection (42-45). To investigate whether H2AS15ph may affect
193 resection, we used an antibody against Rfa1, RPA largest subunit, as a proxy for the ssDNA
194 generated by resection, in ChIP-qPCR at the HO-induced DSB. Interestingly, *H2A-S15E*
195 (phosphorylation mimicking) mutant cells show increased RPA binding near the break, whereas

196 *H2A-S15A* mutant cells behave like wild type (**Fig. 4A**). The *H2A-S129A* cells also show increased
197 RPA signals, reflecting higher ssDNA/resection in this mutant. Double mutants *H2A-S15A/E*
198 *H2A-S129A* have similar increased RPA signals as *H2A-S129A* cells, maybe slightly less than
199 *H2AS15E* cells at some locations (**Fig. 4A**). To confirm that these RPA signals are the
200 consequence of increased DNA end resection, we directly measured by qPCR the DNA signal
201 5kb away from the DSB, compared to an unrelated genomic locus. In this assay, a very
202 significant and similar decrease of signal is detected in *H2A-S15E*, *H2A-S129A* and double
203 mutants, but not in *H2A-S15A* (**Fig. 4B**). These results indicate that H2AS15 phosphorylation
204 leads to increased resection at DSBs, similar to the effect of losing H2AS129 phosphorylation.
205 Furthermore, the effects of each mutant are non-additive, suggesting that they are
206 mechanistically related. An interesting possibility is whether H2AS15ph is also recognized by
207 the BRCT domain of Rad9, this domain being well characterized for its ability to bind
208 H2AS129ph (27). Surprisingly, *in vitro* peptide binding assays with recombinant Rad9 indicate a
209 clear binding preference for the histone H2A tail peptide, but in its non-phosphorylated form
210 (**Fig. 4B**). Importantly, this binding specificity is also confirmed using yeast whole cell extracts in
211 peptide pull-downs and detecting endogenous Rad9 by immunoblotting (**Fig. 4C**). In this case,
212 inducing DNA damage in the cells does not affect endogenous Rad9 ability to bind the H2A
213 peptide *in vitro*. This ability of H2AS15ph to block Rad9 binding to the H2A histone tail may in
214 part explain the increased end resection detected in *H2A-S15E* mutant cells but not in *H2A-*
215 *S15A* (**Fig. 4A-B**). As these results suggest that Rad9 may directly bind histone H2A tail in
216 chromatin *in vivo*, and that H2AS15 phosphorylation may regulate this interaction, we analyze
217 Rad9 binding near the HO-induced DSB by ChIP-qPCR. In wild-type conditions in this specific

218 yeast genetic background, we could only detect Rad9-myc signal by ectopic expression from a
219 plasmid. Furthermore, the specific signal based on the empty vector control could only be
220 detected very close (150bp) on each side of the HO break (**Fig. 4E**). At these locations, Rad9
221 binding is indeed abrogated in the *H2A-S129A* mutant, as expected, and validating the
222 specificity of the signal. In contrast, Rad9 binding does not seem affected by *H2A-S15A/E*
223 mutations. Since H2AS15 phosphorylation occurs more downstream away from the DNA break,
224 the Rad9 signal detected here close to the HO site may not reflect the population regulated by
225 H2AS15ph (see (42, 46) for models of two populations/functions of Rad9/53BP1 near DNA ends
226 versus larger domains). Another possibility is that H2AS15ph is not required for Rad9
227 recruitment but regulates the way it binds nucleosomes and influences end resection.
228 Altogether, these results implicate the DNA damage-induced H2AS15ph histone mark in the
229 regulation of end resection at DSBs.
230

231 **DISCUSSION**

232 Histone tails are sites of various post-translational modifications (PTMs) such as
233 phosphorylation, acetylation, methylation, ubiquitylation and SUMOylation. These
234 modifications are recognized by reader proteins containing specialized domains such as
235 ubiquitin binding domains, BRCT and FHA domains that bind phosphorylation, Chromodomains,
236 MBT domains, Bromodomains and PHD fingers that recognize methylation or acetylation.
237 Proteins and protein complexes use these interactions for their proper recruitment, retention
238 and/or orientation at the target sites to carry out their respective functions (47, 48).

239 In this study, we characterized yeast H2AS15ph as a novel histone modification in the
240 context of DNA damage. This modification is induced in the presence of DNA damaging agent
241 MMS, which is a known alkylating agent and produces DSBs as cells replicate their DNA in S-
242 phase. A large-scale proteomic study had identified H2AS15ph by mass spectrometry and
243 implicated Mec1^{ATR} for its detection (29). Using *in vivo* analysis, we show that indeed Mec1, and
244 not Tel1, is responsible for the induction of this mark around DNA breaks, unlike γ-H2A
245 (H2AS129ph) which is deposited by either Tel1 or Mec1 (**Fig. 3**). While the spreading of γ-H2A
246 at DSBs is not affected in *H2A-S15A/E* mutant cells, the *H2A-S129A* mutant does affect the
247 levels of H2AS15ph (**Fig. 1C-D, 2F**). Furthermore, a decrease of chromatin acetylation is
248 detected in *H2A-S15A/E* mutant cells near the DNA break (**Fig. 1F-G**). We know from previous
249 studies that acetylation of histone H4 and H2A by the NuA4 complex plays an important role for
250 the recruitment of various chromatin remodelers like INO80, RSC and SWI/ SNF required for
251 repair by HR (12, 49-51). Future work will be needed to determine if H2AS15 affects the
252 recruitment of these remodelers.

253 A most interesting finding reported here argues that yeast H2AS15ph corresponds to an
254 evolutionary conserved regulatory function to regulate 53BP1/Rad9 binding to the H2A tail and
255 DNA end resection. The yeast H2AS15 residue seems the functional homolog of mammalian
256 H2AK15 in modulating resection which in turn affects DNA repair pathway selection, albeit
257 through different PTMs. In mammals, when 53BP1 binds H2AK15ub in the vicinity of DSBs, it
258 inhibits resection and favors the NHEJ pathway. This binding inhibits TIP60-mediated
259 acetylation of H4 and H2A tails in chromatin, including H2AK15, which otherwise would block
260 ubiquitylation by RNF168 and 53BP1 binding, favoring resection and HR (25). *H2A-S15E* mutant

261 cells show increased resection, as seen with *H2A-S129A* mutant cells where Rad9^{53BP1} is
262 incapable to bind and inhibit or slow down resection (**Fig. 4A-B**). *In vitro* data suggest that Rad9
263 binds the H2A N-terminal tail in its unmodified state and this binding is abolished when H2AS15
264 is phosphorylated (**Fig. 4C-D**). On the other hand, this regulated interaction does not seem to
265 affect Rad9 recruitment to the DSB (**Fig. 4E**). Since Rad9 is recruited to nucleosomes near DSBs
266 though bivalent interaction with H2AS129ph and H3K79me, our results suggest that Rad9
267 interaction with the H2A tail is not required for its recruitment but can regulate its function
268 linked to DNA end resection. 53BP1 also interacts with nucleosomes through three interfaces,
269 i.e. H2AK15ub-UDR, H4K20me-Tudor and H2A.XS139ph-BRCT. But, as in yeast, only two are
270 required for its binding to nucleosomes, γH2AX-BRCT being dispensable (24, 46, 52). We
271 proposed a model depicted in (Fig. 4F) where resection of DNA ends produces ssDNA which
272 gets coated by RPA and recruits Mec1^{ATR} through its binding partner Lcd1/Ddc2^{ATRIP} (34, 36).
273 Mec1 then phosphorylates H2AS15 which inhibits Rad9 function and therefore increases
274 resection. H2AS15ph may be a dynamic mark, switching between phosphorylation and non-
275 phosphorylation states to fine-tune the process of resection. This conserved function of the
276 H2A tail to regulate Rad9/53BP1 binding and resection is even further supported by a recent
277 report showing phosphorylation of the ubiquitin moiety of H2AK15ub (H2AK15pUbT12) to
278 inhibit 53BP1 binding and favor resection (53).

279 Future work will address whether specific proteins may bind H2AS15ph. While our
280 peptide pull-downs with yeast extracts followed by mass spectrometry did not yield clear
281 results (data not shown), we speculate that other DNA repair proteins such as Rtt107 and
282 Dpb11 which have BRCT domains could recognize H2AS15ph. Rtt107 was recently shown to

283 bind H4T80ph and γ-H2A to counteract Rad9-modulated checkpoint activity (54). Dpb11 has
284 been shown to act as a scaffold protein for various checkpoint proteins and is involved in Rad9
285 recruitment/retention at DSBs (55, 56). H2AS15 may also act redundantly with other DNA
286 damage induced histone phosphorylation marks and function as a scaffold for proper
287 orientation or retention of repair factors.
288

289 **MATERIAL AND METHODS**

290 **Yeast strains**

291 All yeast strains used in the current study are from FY406 (57) and JKM179 (58) (*hta1-*
292 *htb1Δ::NatMX* , *hta2-htb2Δ::KANMX*) backgrounds with deletion of both copies of H2A and H2B
293 genes. These strains carry an ectopic copy of *HTA1-HTB1* on low copy vector pRS413 (in FY406)
294 or pRS414 (in JKM179). Gene deletion and point mutations were obtained through standard
295 PCR techniques. Plasmid shuffling using 5-Fluoroorotic acid (5-FOA) was used to introduce the
296 plasmid with point mutations in respective backgrounds. Yeast background JKM139 (58) with
297 deletion of *sml1Δ::NATMX* , *lcd1Δ::KANMX* , *xrs2Δ::TRP1* was used in this study. QY362
298 (JKM139 *RAD9-13MYC::KANMX*) was used for peptide pull down experiments while the Rad9-
299 myc ChIP-qPCR were done in the JKM179 background with *HTA1/2-HTB1/2* deletions covered
300 wild type or mutant H2A and ectopic Rad9-Myc expression from a pRS315 vector (40). General
301 lithium acetate method was used to transform the yeast cells. Cells were grown in YPD (1%
302 yeast extract, 2% peptone, 2% dextrose) at 30°C until early log phase. For spot assay 1:10
303 dilution of the culture was spotted and grown at 30°C for 3-4 days.

304 **Chromatin Immunoprecipitation (ChIP)**

305 ChIP-qPCR was performed as described previously (59). In brief, cells were grown overnight in
306 YP-Raffinose until OD_{600} of 0.5-1, at this point galactose (2%) was added to induced DSB at *MAT*
307 locus for 3 hours. This was followed by cross-linking of cells with formaldehyde and lysing with
308 bead-beater. Sonication was performed on Diagenode Bioruptor to obtain chromatin size of
309 ~200-500bp. 100μg of chromatin was used to setup the immunoprecipitation reaction with
310 anti-H2A-S129ph (Upstate 07-745), anti-H2A-S15Ph (antibody was produced in rabbit using the

311 peptide sequence: Ac-GSAAKA(pS)QSRSAK-C. Affinity purification was performed to improve
312 the specificity of the antibody, with phosphorylated versus non-phosphorylated peptides.
313 Antibody was produced by Thermo Fisher Scientific), anti-Rfa1 (Agrisera AS07214), anti-H4ac
314 (Upstate 06-946), anti-H4 (Abcam 7311) and anti-Myc (9E10 Babco MMS150R) and reaction
315 was allowed to mix on a wheel overnight at 4°C. Next morning Protein-A agarose beads
316 (protein-G magnetic beads for anti-Myc) were added followed by additional 3-4 hours on a
317 wheel at 4°C. After multiple washing steps the DNA was eluted and incubated at 65°C overnight
318 for de-cross linking followed by phenol-chloroform extraction of DNA. This DNA was
319 resuspended in NTE and used for qPCR. LC480 LightCycler (Roche) was used to quantify DNA
320 with the primer pairs as mentioned in the respective figures to calculate % of
321 immunoprecipitation (IP)/ input. The data represents mean of two independent biological
322 replicates. Error bars indicate the ranges between the two biological replicates. Fold
323 enrichment represents ratio of %IP/input at indicated loci around DSB normalized on signal at
324 negative-control locus IntergenicV. Levels of HO-induced DNA break was verified by qPCR
325 across the HO cut-site (normalized on control locus) and were similar in all experiments. Direct
326 measurement of end resection by qPCR was done using primers 4.8kb left of the HO cut-site
327 and presented as a ratio of signal over a control locus (*PRE1*, (60)). Primer sequences are
328 available upon request.

329 **Purification of native yeast chromatin**

330 Native yeast chromatin was prepared as described previously (61), cells were treated with MMS
331 (0.05%) or DMSO (control) for 2 hours to induce DNA damage. Lambda protein phosphatase
332 (λPP) (NEB) was used to dephosphorylate the purified chromatin. The reaction mixture was

333 incubated for 30 mins at 30°C followed by booster of λPP and additional incubation for 30 mins
334 at 30°C.

335 **Recombinant protein purification**

336 Recombinant Rad9 (C-terminal containing Tudor and BRCT domains) protein was purified as
337 described previously (62). In short, bacterial cells were grown overnight at 16°C with IPTG
338 induction. Next day cells were lysed with lysozyme followed by sonication. The soluble portion
339 was incubated with glutathione sepharose (GE healthcare) beads for 3-4 hours at 4°C and
340 eluted with glutathione. The eluted protein concentration was quantified by running on SDS-
341 PAGE with known BSA standards followed by coomassie staining.

342 **Peptide-pull down**

343 Peptide-pull down was performed with synthetic peptide corresponding to H2A N-terminal (aa
344 1-23) obtained from AnaSpec. 1μg of peptide was incubated with 1μg of GST-tagged protein
345 overnight on wheel at 4°C in binding buffer (50 mM Tris–HCl pH 7.5, 50 mM NaCl, 0.1% NP-40, 1
346 mM PMSF and phosphatase inhibitors). Next morning streptavidin dynabeads were added to
347 the reaction mixture and kept at 4°C for two additional hours followed by washing, running on
348 SDS-PAGE and western blotting with anti-GST (Sigma G1160).

349 Peptide-pull downs with yeast cell extracts were performed by growing cells in YPD and treating
350 with MMS (0.05%) or DMSO for 2 hours (final OD_{600} ~1.0-1.5). Cells were centrifuged, the pellet
351 was washed with cold milliQ water, resuspended in sensitization buffer (100mM Tris-HCl pH
352 9.4, 10mM DTT) and incubated at 30°C on a wheel for 15 mins. It was then centrifuged at 500g
353 for 5mins at 4°C, resuspended in 30ml of spheroplasting buffer (1.2M Sorbitol 20mM Hepes pH
354 7.5), centrifuged again, resuspended in 40ml of spheroplasting buffer with lyticase and

355 incubated on wheel at 30°C for 90 mins. After centrifugation at 500g for 5 mins, wash with
356 wash buffer (1.2M Sorbitol, 20mM Pipes pH 6.4, 1mM $MgCl_2$), it was resuspended in 25ml of
357 nuclear isolation buffer; NIB (250mM Sucrose, 60mM KCl, 1mM PMSF, 14mM NaCl, 0.8% Triton
358 X-100, 5mM $MgCl_2$, 1mM $CaCl_2$, 15mM MES), mixed well to remove clumps and kept on ice for
359 20 mins. After centrifugation and two washes with NIB (until white nuclear pellet was
360 obtained), the pellet was resuspended in pull-down buffer (400mM NaCl, 1mM PMSF, 50mM
361 Tris-HCl pH8, 0.5% NP-40, 5 mM β-glycerophosphate, 10 mM sodium butyrate, 5 mM NaF) to
362 get 300mM NaCl in the final volume, followed by incubation on rotating plate at 4°C for 20
363 mins. After centrifugation at 14,000rpm at 4°C for 30 mins, the supernatant was collected
364 (nuclear extract). Biotinylated peptides were bound to streptavidin dynabeads in peptide
365 binding buffer (150mM NaCl, 50mM Tris-HCl pH8.0, 0.1% NP-40, 5 mM β-glycerophosphate, 10
366 mM sodium butyrate, 5 mM NaF) by incubating at room temperature on wheel for 30 mins.
367 Peptide-dynabeads were washed with protein binding buffer (140mM NaCl, 50mM Tris-HCl pH
368 8.0, 0.1% NP-40, 0.5mM DTT, 10μM $ZnCl_2$, 5 mM β-glycerophosphate, 10 mM sodium butyrate,
369 5 mM NaF) followed by addition of 600μg of nuclear extract to each pull-down reaction and
370 incubated at 4°C on wheel for 2 hours. Nuclear extract that was incubated with phospho
371 peptide was initially incubated with non-phospho peptide, on the other hand, nuclear extract
372 for non-phospho peptide was initially incubated with phospho peptide for 2 hours at 4°C on
373 wheel. After 3-4 washed with final wash buffer (350mM NaCl, 50mM Tris-HCl pH8.0, 0.1% NP-
374 40, 0.5mM DTT, 10μM $ZnCl_2$, 5 mM β-glycerophosphate, 10 mM sodium butyrate, 5 mM NaF),
375 Laemmli buffer was added, boiled and resolved in SDS-PAGE followed by western blotting with
376 anti-Myc (9E10 Babco MMS150R).

377

378 ***Acknowledgments***

379 We thank Xue Cheng for important advice. We are grateful to Jim Haber for sharing
380 reagents/strains and stimulating discussions. This work was supported by a grant from the
381 Canadian Institutes of Health Research (CIHR) to J.C. (FDN-143314). S.A. held a
382 Desjardins/Fondation du CHU de Québec studentship. J.C. holds the Canada Research Chair in
383 Chromatin Biology and Molecular Epigenetics.

384

385

386 **REFERENCES**

387 1. Hanahan D, Weinberg RA. 2011. Hallmarks of cancer: the next generation. Cell 144:646-
388 74.
389 2. Jackson SP, Bartek J. 2009. The DNA-damage response in human biology and disease.
390 Nature 461:1071-8.
391 3. Chiruvella KK, Liang Z, Wilson TE. 2013. Repair of double-strand breaks by end joining.
392 Cold Spring Harb Perspect Biol 5:a012757.
393 4. Symington LS. 2016. Mechanism and regulation of DNA end resection in eukaryotes. Crit
394 Rev Biochem Mol Biol 51:195-212.
395 5. Abraham RT. 2001. Cell cycle checkpoint signaling through the ATM and ATR kinases.
396 Genes Dev 15:2177-96.
397 6. Smith GC, Jackson SP. 1999. The DNA-dependent protein kinase. Genes & development
398 13:916-934.
399 7. Downs JA, Lowndes NF, Jackson SP. 2000. A role for Saccharomyces cerevisiae histone
400 H2A in DNA repair. Nature 408:1001-1004.
401 8. Paull TT, Rogakou EP, Yamazaki V, Kirchgessner CU, Gellert M, Bonner WM. 2000. A
402 critical role for histone H2AX in recruitment of repair factors to nuclear foci after DNA
403 damage. Current Biology 10:886-895.
404 9. Rogakou EP, Boon C, Redon C, Bonner WM. 1999. Megabase Chromatin Domains
405 Involved in DNA Double-Strand Breaks in Vivo. The Journal of Cell Biology 146:905-916.
406 10. Lee CS, Lee K, Legube G, Haber JE. 2014. Dynamics of yeast histone H2A and H2B
407 phosphorylation in response to a double-strand break. Nat Struct Mol Biol 21:103-9.
408 11. Shroff R, Arbel-Eden A, Pilch D, Ira G, Bonner WM, Petrini JH, Haber JE, Lichten M. 2004.
409 Distribution and dynamics of chromatin modification induced by a defined DNA double-
410 strand break. Curr Biol 14:1703-11.

411 12. Downs JA, Allard S, Jobin-Robitaille O, Javaheri A, Auger A, Bouchard N, Kron SJ, Jackson
412 SP, Côté J. 2004. Binding of Chromatin-Modifying Activities to Phosphorylated Histone
413 H2A at DNA Damage Sites. Molecular Cell 16:979-990.
414 13. Morrison AJ, Highland J, Krogan NJ, Arbel-Eden A, Greenblatt JF, Haber JE, Shen X. 2004.
415 INO80 and gamma-H2AX interaction links ATP-dependent chromatin remodeling to DNA
416 damage repair. Cell 119:767-75.
417 14. van Attikum H, Fritsch O, Gasser SM. 2007. Distinct roles for SWR1 and INO80 chromatin
418 remodeling complexes at chromosomal double-strand breaks. EMBO J 26:4113-25.
419 15. van Attikum H, Fritsch O, Hohn B, Gasser SM. 2004. Recruitment of the INO80 complex
420 by H2A phosphorylation links ATP-dependent chromatin remodeling with DNA double-
421 strand break repair. Cell 119:777-88.
422 16. Dantuma NP, van Attikum H. 2016. Spatiotemporal regulation of posttranslational
423 modifications in the DNA damage response. The EMBO Journal 35:6-23.
424 17. Wysocki R, Javaheri A, Allard S, Sha F, Côté J, Kron SJ. 2005. Role of Dot1-Dependent
425 Histone H3 Methylation in G₁ and S Phase DNA Damage Checkpoint
426 Functions of Rad9. Molecular and Cellular Biology 25:8430-8443.
427 18. Celeste A, Petersen S, Romanienko PJ, Fernandez-Capetillo O, Chen HT, Sedelnikova OA,
428 Reina-San-Martin B, Coppola V, Meffre E, Difilippantonio MJ, Redon C, Pilch DR, Olaru A,
429 Eckhaus M, Camerini-Otero RD, Tessarollo L, Livak F, Manova K, Bonner WM,
430 Nussenzweig MC, Nussenzweig A. 2002. Genomic Instability in Mice Lacking Histone
431 H2AX. Science 296:922-927.
432 19. Cheung WL, Turner FB, Krishnamoorthy T, Wolner B, Ahn SH, Foley M, Dorsey JA,
433 Peterson CL, Berger SL, Allis CD. 2005. Phosphorylation of histone H4 serine 1 during
434 DNA damage requires casein kinase II in S. cerevisiae. Curr Biol 15:656-60.
435 20. Utley RT, Lacoste N, Jobin-Robitaille O, Allard S, Cote J. 2005. Regulation of NuA4
436 histone acetyltransferase activity in transcription and DNA repair by phosphorylation of
437 histone H4. Mol Cell Biol 25:8179-90.
438 21. Harvey AC, Jackson SP, Downs JA. 2005. Saccharomyces cerevisiae histone H2A Ser122
439 facilitates DNA repair. Genetics 170:543-53.
440 22. Krishnamoorthy T, Chen X, Govin J, Cheung WL, Dorsey J, Schindler K, Winter E, Allis CD,
441 Guacci V, Khochbin S, Fuller MT, Berger SL. 2006. Phosphorylation of histone H4 Ser1
442 regulates sporulation in yeast and is conserved in fly and mouse spermatogenesis.
443 Genes & development 20:2580-2592.
444 23. House NCM, Polleys EJ, Quasem I, De la Rosa Mejia M, Joyce CE, Takacsi-Nagy O, Krebs
445 JE, Fuchs SM, Freudenreich CH. 2019. Distinct roles for S. cerevisiae H2A copies in
446 recombination and repeat stability, with a role for H2A.1 threonine 126. eLife 8:e53362.
447 24. Fradet-Turcotte A, Canny MD, Escribano-Díaz C, Orthwein A, Leung CC, Huang H, Landry
448 MC, Kitevski-LeBlanc J, Noordermeer SM, Sicheri F, Durocher D. 2013. 53BP1 is a reader
449 of the DNA-damage-induced H2A Lys 15 ubiquitin mark. Nature 499:50-4.
450 25. Jacquet K, Fradet-Turcotte A, Avvakumov N, Lambert JP, Roques C, Pandita RK, Paquet E,
451 Herst P, Gingras AC, Pandita TK, Legube G, Doyon Y, Durocher D, Côté J. 2016. The TIP60
452 Complex Regulates Bivalent Chromatin Recognition by 53BP1 through Direct H4K20me
453 Binding and H2AK15 Acetylation. Mol Cell 62:409-421.

454 26. Grenon M, Costelloe T, Jimeno S, O'Shaughnessy A, FitzGerald J, Zgheib O, Degerth L,
455 Lowndes NF. 2007. Docking onto chromatin via the Saccharomyces cerevisiae Rad9
456 Tudor domain. Yeast 24:105-119.
457 27. Hammet A, Magill C, Heierhorst J, Jackson SP. 2007. Rad9 BRCT domain interaction with
458 phosphorylated H2AX regulates the G1 checkpoint in budding yeast. EMBO Rep 8:851-7.
459 28. Javaheri A, Wysocki R, Jobin-Robitaille O, Altaf M, Cote J, Kron SJ. 2006. Yeast G1 DNA
460 damage checkpoint regulation by H2A phosphorylation is independent of chromatin
461 remodeling. Proc Natl Acad Sci U S A 103:13771-6.
462 29. Bastos de Oliveira FM, Kim D, Cussiol JR, Das J, Jeong MC, Doerfler L, Schmidt KH, Yu H,
463 Smolka MB. 2015. Phosphoproteomics reveals distinct modes of Mec1/ATR signaling
464 during DNA replication. Mol Cell 57:1124-1132.
465 30. Allard S, Utley RT, Savard J, Clarke A, Grant P, Brandl CJ, Pillus L, Workman JL, Côté J.
466 1999. NuA4, an essential transcription adaptor/histone H4 acetyltransferase complex
467 containing Esa1p and the ATM-related cofactor Tra1p. The EMBO Journal 18:5108-5119.
468 31. Redon C, Pilch DR, Rogakou EP, Orr AH, Lowndes NF, Bonner WM. 2003. Yeast histone
469 2A serine 129 is essential for the efficient repair of checkpoint-blind DNA damage.
470 EMBO reports 4:678-684.
471 32. Nakada D, Matsumoto K, Sugimoto K. 2003. ATM-related Tel1 associates with double-
472 strand breaks through an Xrs2-dependent mechanism. Genes Dev 17:1957-62.
473 33. Oh J, Al-Zain A, Cannavo E, Cejka P, Symington LS. 2016. Xrs2 Dependent and
474 Independent Functions of the Mre11-Rad50 Complex. Mol Cell 64:405-415.
475 34. Zou L, Elledge SJ. 2003. Sensing DNA Damage Through ATRIP Recognition of RPA-ssDNA
476 Complexes. Science 300:1542-1548.
477 35. Li K, Bronk G, Kondev J, Haber JE. 2020. Yeast ATM and ATR kinases use different
478 mechanisms to spread histone H2A phosphorylation around a DNA double-strand break.
479 Proceedings of the National Academy of Sciences 117:21354-21363.
480 36. Gobbini E, Cesena D, Galbiati A, Lockhart A, Longhese MP. 2013. Interplays between
481 ATM/Tel1 and ATR/Mec1 in sensing and signaling DNA double-strand breaks. DNA
482 Repair (Amst) 12:791-9.
483 37. Paciotti V, Clerici M, Lucchini G, Longhese MP. 2000. The checkpoint protein Ddc2,
484 functionally related to S. pombe Rad26, interacts with Mec1 and is regulated by Mec1-
485 dependent phosphorylation in budding yeast. Genes & Development 14:2046-2059.
486 38. Chen X, Cui D, Papusha A, Zhang X, Chu CD, Tang J, Chen K, Pan X, Ira G. 2012. The Fun30
487 nucleosome remodeller promotes resection of DNA double-strand break ends. Nature
488 489:576-80.
489 39. Eapen VV, Sugawara N, Tsabar M, Wu WH, Haber JE. 2012. The Saccharomyces
490 cerevisiae chromatin remodeler Fun30 regulates DNA end resection and checkpoint
491 deactivation. Mol Cell Biol 32:4727-40.
492 40. Nnakwe CC, Altaf M, Cote J, Kron SJ. 2009. Dissection of Rad9 BRCT domain function in
493 the mitotic checkpoint response to telomere uncapping. DNA Repair (Amst) 8:1452-61.
494 41. Toh GW, O'Shaughnessy AM, Jimeno S, Dobbie IM, Grenon M, Maffini S, O'Rorke A,
495 Lowndes NF. 2006. Histone H2A phosphorylation and H3 methylation are required for a
496 novel Rad9 DSB repair function following checkpoint activation. DNA Repair (Amst)
497 5:693-703.

498 42. Ferrari M, Dibitetto D, De Gregorio G, Eapen VV, Rawal CC, Lazzaro F, Tsabar M, Marini
499 F, Haber JE, Pellicioli A. 2015. Functional interplay between the 53BP1-ortholog Rad9
500 and the Mre11 complex regulates resection, end-tethering and repair of a double-strand
501 break. PLoS Genet 11:e1004928.
502 43. Escribano-Díaz C, Orthwein A, Fradet-Turcotte A, Xing M, Young JT, Tkáč J, Cook MA,
503 Rosebrock AP, Munro M, Canny MD, Xu D, Durocher D. 2013. A cell cycle-dependent
504 regulatory circuit composed of 53BP1-RIF1 and BRCA1-CtIP controls DNA repair pathway
505 choice. Mol Cell 49:872-83.
506 44. Noordermeer SM, Adam S, Setiaputra D, Barazas M, Pettitt SJ, Ling AK, Olivieri M,
507 Alvarez-Quilon A, Moatti N, Zimmermann M, Annunziato S, Krastev DB, Song F,
508 Brandsma I, Frankum J, Brough R, Sherker A, Landry S, Szilard RK, Munro MM, McEwan
509 A, Goullet de Rugy T, Lin ZY, Hart T, Moffat J, Gingras AC, Martin A, van Attikum H,
510 Jonkers J, Lord CJ, Rottenberg S, Durocher D. 2018. The shieldin complex mediates
511 53BP1-dependent DNA repair. Nature 560:117-121.
512 45. Zimmermann M, Lottersberger F, Buonomo SB, Sfeir A, de Lange T. 2013. 53BP1
513 Regulates DSB Repair Using Rif1 to Control 5' End Resection. Science 339:700-704.
514 46. Bothmer A, Robbiani DF, Di Virgilio M, Bunting SF, Klein IA, Feldhahn N, Barlow J, Chen
515 HT, Bosque D, Callen E, Nussenzweig A, Nussenzweig MC. 2011. Regulation of DNA end
516 joining, resection, and immunoglobulin class switch recombination by 53BP1. Mol Cell
517 42:319-29.
518 47. Wilson MD, Durocher D. 2017. Reading chromatin signatures after DNA double-strand
519 breaks. Philos Trans R Soc Lond B Biol Sci 372.
520 48. Rossetto D, Truman AW, Kron SJ, Cote J. 2010. Epigenetic modifications in double-strand
521 break DNA damage signaling and repair. Clin Cancer Res 16:4543-52.
522 49. Bennett G, Peterson CL. 2015. SWI/SNF recruitment to a DNA double-strand break by
523 the NuA4 and Gcn5 histone acetyltransferases. DNA Repair 30:38-45.
524 50. House NCM, Yang JH, Walsh SC, Moy JM, Freudenreich CH. 2014. NuA4 initiates dynamic
525 histone H4 acetylation to promote high-fidelity sister chromatid recombination at
526 postreplication gaps. Mol Cell 55:818-828.
527 51. Cheng X, Cote V, Cote J. 2021. NuA4 and SAGA acetyltransferase complexes cooperate
528 for repair of DNA breaks by homologous recombination. PLoS Genet 17:e1009459.
529 52. Zgheib O, Pataky K, Brugger J, Halazonetis TD. 2009. An oligomerized 53BP1 tudor
530 domain suffices for recognition of DNA double-strand breaks. Mol Cell Biol 29:1050-8.
531 53. Walser F, Mulder MPC, Bragantini B, Burger S, Gubser T, Gatti M, Botuyan MV, Villa A,
532 Altmeyer M, Neri D, Ovaa H, Mer G, Penengo L. 2020. Ubiquitin Phosphorylation at
533 Thr12 Modulates the DNA Damage Response. Molecular Cell 80:423-436.e9.
534 54. Millan-Zambrano G, Santos-Rosa H, Puddu F, Robson SC, Jackson SP, Kouzarides T. 2018.
535 Phosphorylation of Histone H4T80 Triggers DNA Damage Checkpoint Recovery. Mol Cell
536 72:625-635 e4.
537 55. Liu Y, Cussiol JR, Dibitetto D, Sims JR, Twayana S, Weiss RS, Freire R, Marini F, Pellicioli A,
538 Smolka MB. 2017. TOPBP1(Dpb11) plays a conserved role in homologous recombination
539 DNA repair through the coordinated recruitment of 53BP1(Rad9). J Cell Biol 216:623-
540 639.

541 56. Granata M, Lazzaro F, Novarina D, Panigada D, Puddu F, Abreu CM, Kumar R, Grenon M,
542 Lowndes NF, Plevani P, Muzi-Falconi M. 2010. Dynamics of Rad9 chromatin binding and
543 checkpoint function are mediated by its dimerization and are cell cycle-regulated by
544 CDK1 activity. PLoS Genet 6:e1001047.
545 57. Hirschhorn JN, Bortvin AL, Ricupero-Hovasse SL, Winston F. 1995. A new class of histone
546 H2A mutations in Saccharomyces cerevisiae causes specific transcriptional defects in
547 vivo. Molecular and Cellular Biology 15:1999-2009.
548 58. Lee SE, Moore JK, Holmes A, Umezu K, Kolodner RD, Haber JE. 1998.
549 Saccharomyces Ku70, Mre11/Rad50, and RPA Proteins Regulate Adaptation
550 to G2/M Arrest after DNA Damage. Cell 94:399-409.
551 59. Rossetto D, Cramet M, Wang AY, Steunou AL, Lacoste N, Schulze JM, Cote V, Monnet-
552 Saksouk J, Piquet S, Nourani A, Kobor MS, Cote J. 2014. Eaf5/7/3 form a functionally
553 independent NuA4 submodule linked to RNA polymerase II-coupled nucleosome
554 recycling. EMBO J 33:1397-415.
555 60. Mojumdar A, Sorenson K, Hohl M, Toulouze M, Lees-Miller SP, Dubrana K, Petrini JHJ,
556 Cobb JA. 2019. Nej1 Interacts with Mre11 to Regulate Tethering and Dna2 Binding at
557 DNA Double-Strand Breaks. Cell Reports 28:1564-1573.e3.
558 61. Altaf M, Utley RT, Lacoste N, Tan S, Briggs SD, Cote J. 2007. Interplay of chromatin
559 modifiers on a short basic patch of histone H4 tail defines the boundary of telomeric
560 heterochromatin. Mol Cell 28:1002-14.
561 62. Setiaputra D, Ahmad S, Dalwadi U, Steunou A-L, Lu S, Ross JD, Dong M-Q, Côté J, Yip CK.
562 2018. Molecular Architecture of the Essential Yeast Histone Acetyltransferase Complex
563 NuA4 Redefines Its Multimodularity. Molecular and Cellular Biology 38:e00570-17.
564

565

566 **FIGURE LEGENDS**

567 **Fig 1: *H2A-S15* mutants are sensitive to DNA damage and functions independently of γ-H2A.**

568 (A) Sequence of H2A N-termini highlighting the SQ site at position 15 in *S. cerevisiae* and
569 corresponding lysine at position 15 in *H. sapiens*.

570 (B, C) Phenotypic analysis of yeast cells expressing wild type or the indicated H2A mutants. Ten-
571 fold serial dilutions of log phase cells were spotted on plates containing rich media alone or in
572 presence of DNA damaging agent methylmethane sulfonate (MMS). *H2A-S15E* showed a slight
573 growth defect in presence of the drug. Whereas, both *H2A-S15A/E* in background with *H2A-*
574 *S129A* showed stronger sensitivity than their respective single mutants. *H2B-T129A* did not
575 influence the growth of *H2A-S15A/E*.

576 (D, E) ChIP-qPCR showing γ-H2A at an inducible DSB is not affected by *H2A-S15A/E*. Cells were
577 grown in YP-raffinose overnight till log phase followed by addition of galactose to induce DSB
578 for 3 hours before cross-linking the chromatin. Primer pairs used flanked the DNA sequence on
579 both left and right side at 3Kb, 7Kb and 10Kb of the DSB at *MAT* locus. Anti-H4 signal was used
580 to normalize for histone occupancy. The data represents mean of two independent biological
581 replicates. Error bars indicate the range between the two biological replicates.

582 (F) *H2A-S15A/E* affects the acetylation of histone H4 and H2A. Western blot analysis of yeast
583 whole cell extracts (WCE) with anti-H4ac reveals a slight reduction in H4ac and H2Aac in *H2A-*
584 *S15A* and to a lesser extent in *H2A-S15E* compared to wild type. Histone H3 was used as loading
585 control.

586 (G) *H2A-S15A/ E* show reduced H4ac signal in regions close to the DNA break site. Signal for
587 H4ac was normalized for histone occupancy on total H4 signal. ChIP-qPCR was performed as
588 described in (D), with primers flanking 150bp, 1kb, 3Kb left and 0.5Kb, 1kb, 3Kb right of DSB.
589

590 **Fig 2: H2AS15ph is locally induced upon DNA double strand break formation and spread over**
591 **several kilobases.**

592 (A) H2AS15ph signal increased when yeast cells are treated with DNA damaging agent, MMS.
593 Western blot analysis was performed with 300ng of native chromatin purified from yeast cells
594 treated with DMSO (untreated control) or MMS. Anti-H2AS129ph was used as positive control
595 for the MMS treatment. Antibodies against histone H2B and H4 were used as loading control.

596 (B) Anti-H2AS15ph is specific for recognizing a phosphorylation mark on H2A. Western blot
597 analysis was performed with 300ng of native chromatin purified form MMS-treated yeast cells
598 after incubation with or without lambda protein phosphatase (λPP). Lane with λPP treatment
599 showed a significant decrease in signal for H2A-S15ph. Histone H4 was used as loading control.

600 (C) H2AS15ph spreads on both sides of the HO endonuclease-induced single DSB at the *MAT*
601 locus. Signal for H2AS15ph showed enrichment after the induction of the DSB in wild type but
602 not in *H2A-S15A*. ChIP-qPCR was performed as described in Figure 1D. Fold enrichment was
603 calculated as ratio of %IP/ input normalized on total H4 for histone occupancy at indicated loci
604 around the DSB to the signal at the negative control locus intergenicV.

605 (D, E) Kinetics of H2S15ph and H2AS129ph accumulation after the induction of the HO DSB.
606 ChIP samples were analyzed after 0, 30min, 1hr and 3hrs of HO induction. Anti-H4 signal was
607 used to normalize for histone occupancy. Enrichments were measured as described in (C).

608 (F) Decreased H2AS15ph signals in cells lacking γH2A. ChIP-qPCR of H2AS15ph before and after
609 HO induction in wild type and *H2A-S129A* mutant cells. Enrichments were measured as
610 described in (C).
611
612 **Fig 3: Mec1^{ATR} mediates phosphorylation of H2AS15 *in vivo*.**
613 (A) Phosphorylation of H2AS129 carried out by Mec1^{ATR} and Tel1^{ATM}. Signal for H2AS129ph at
614 DSB in *lcd1*Δ (loss of Mec1) is similar to wild type proximal to the break but much reduced distal
615 to the break. H2AS129ph signal is abolished in *lcd1*Δ*xrs2*Δ (loss of Mec1 and Tel1). The line
616 representing the signal for GAL *lcd1*Δ*xrs2*Δ is hidden behind since it has similar values as
617 uninduced/raffinose samples.
618 (B) Phosphorylation of H2AS15 is only mediated by Mec1^{ATR}. Loss of H2AS15ph signal in *lcd1*Δ
619 and *lcd1*Δ*xrs2*Δ compared to WT.
620 All yeast stains used in the above experiments have *sml1*Δ background. ChIP-qPCR was
621 performed as described in Figure 1D, primer pairs flanking 1Kb left and right of DSB were also
622 used.
623
624 **Fig 4: H2AS15 regulates resection of DNA ends at DSB and Rad9^{53BP1} binding *in vitro***
625 (A) *H2A-S15E* mutant has increased DNA end resection compared to *H2A-S15A* and wild type
626 backgrounds, as shown by single-strand DNA binding RPA signal. *H2A-S129A* is used as a
627 positive control as it also leads to higher resection/RPA binding. ChIP-qPCR was performed as
628 described in Figure 1D with antibody against Rfa1 (largest RPA subunit) and primer pairs
629 flanking 1Kb, 3Kb and 7Kb left and right of DSB.

630 (B) Increased DNA end resection in the *H2A-S15E* mutant is also confirmed by directly
631 measuring DNA signal loss near the HO DSB. After 3hrs in inducing media, qPCR was used to
632 measure DNA at 4.8kb Left of the HO cut-site and at control locus in the genome (*PRE1*). Signal
633 ratios on the control locus show are decreased in *H2A-S15E* and *H2A-S129A* mutants, indicating
634 similar higher end resection in these cells.
635 (C) Peptide pull-down assay with GST-tagged recombinant Rad9 and indicated H2A N-terminal
636 peptides. rRad9 binds to unmodified peptide over phosphorylated peptide. Empty GST is used
637 as negative control.
638 (D) Peptide pull-down assay as in (B) but using extracts from yeast cells treated or not with
639 MMS and expressing myc-tagged Rad9.
640 (E) Binding of Rad9 close to the HO DSB is not affected by the H2AS15 mutants *in vivo*. ChIP-
641 qPCRs of Rad9-Myc ectopically expressed in the indicated backgrounds show significant binding
642 within 150bp of the break, which is lost in the *H2A-S129A* mutant but not in *H2A-S15E*. An
643 strain with an empty vector (E.V.) is used as control for background non-specific Myc signal.
644 (F) Model for the role H2AS15ph in DSB repair. Mec1 phosphorylates H2AS15 in the region
645 surrounding the DSB. This phosphorylation blocks Rad9 binding to the H2A tail in the bound
646 nucleosomes, which disrupts its function and results in increased resection. H2AS15ph may
647 function as a dynamic switch to modulate resection, phosphorylation enabling resection and
648 non-phosphorylation preventing hyper-resection.
649
650

FIGURE 1

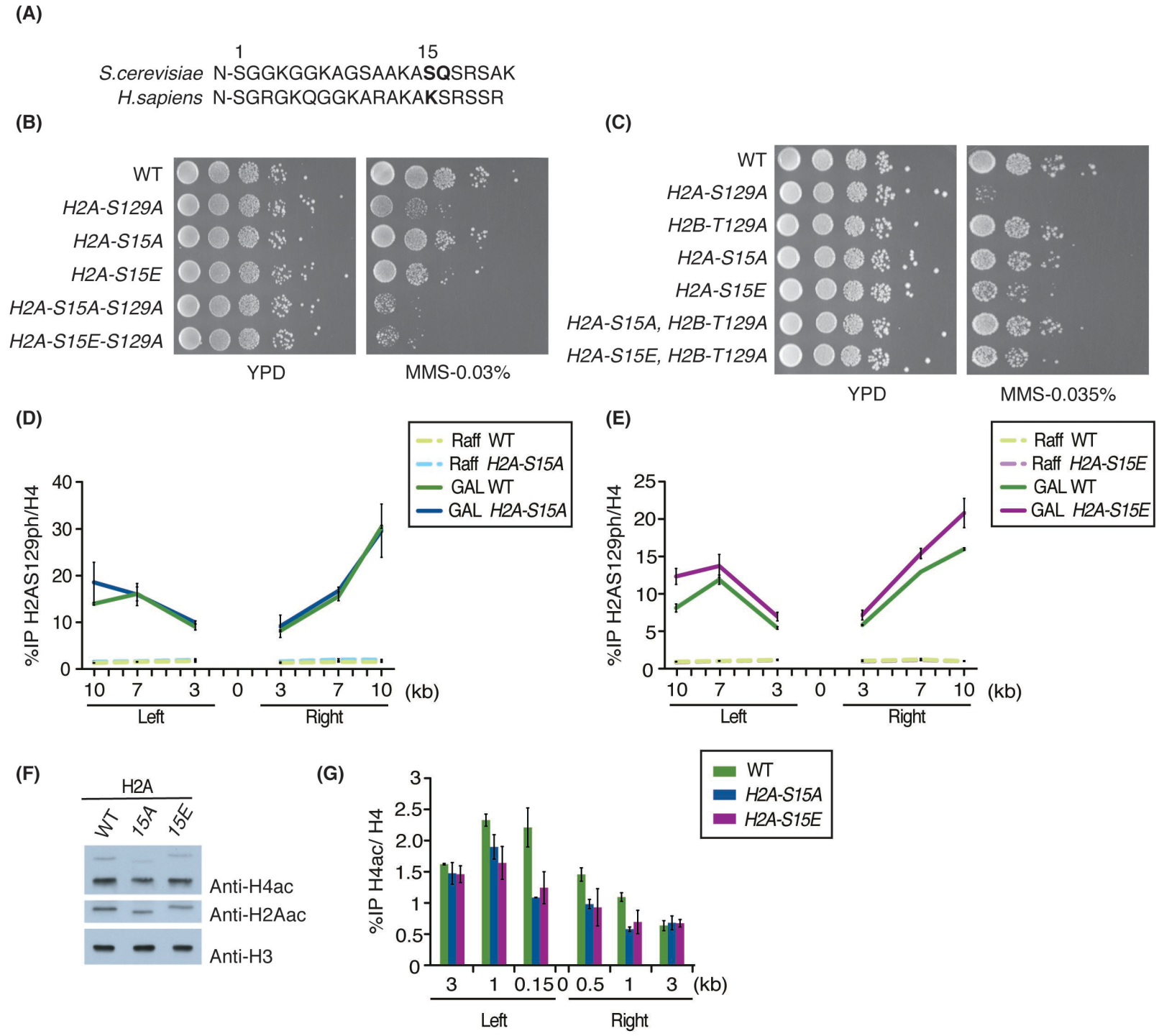
(A)
1
15
S.cerevisiae N-SGGKGGKAGSAAKASQSRSAK
H.sapiens N-SGRGKQGGKARAKAKSRSSR
(B)
WT
H2A-S129A
H2A-S15A
H2A-S15E
H2A-S15A-S129A
H2A-S15E-S129A
YPD
MMS-0.03%
(C)
WT
H2A-S129A
H2B-T129A
H2A-S15A
H2A-S15E
H2A-S15A, H2B-T129A
H2A-S15E, H2B-T129A
YPD
MMS-0.035%
(D)
Raff WT
Raff H2A-S15A
GAL WT
GAL H2A-S15A
%IP H2AS129ph/H4
40
30
20
10
0
10 7 3 0 3 7 10 (kb)
Left
Right
(E)
Raff WT
Raff H2A-S15E
GAL WT
GAL H2A-S15E
%IP H2AS129ph/H4
25
20
15
10
5
0
10 7 3 0 3 7 10 (kb)
Left
Right
(F)
H2A
WT
15A
15E
Anti-H4ac
Anti-H2Aac
Anti-H3
(G)
WT
H2A-S15A
H2A-S15E
%IP H4ac/ H4
3
2.5
2.0
1.5
1
0.5
0
3 1 0.15 0 0.5 1 3 (kb)
Left
Right

FIGURE 2

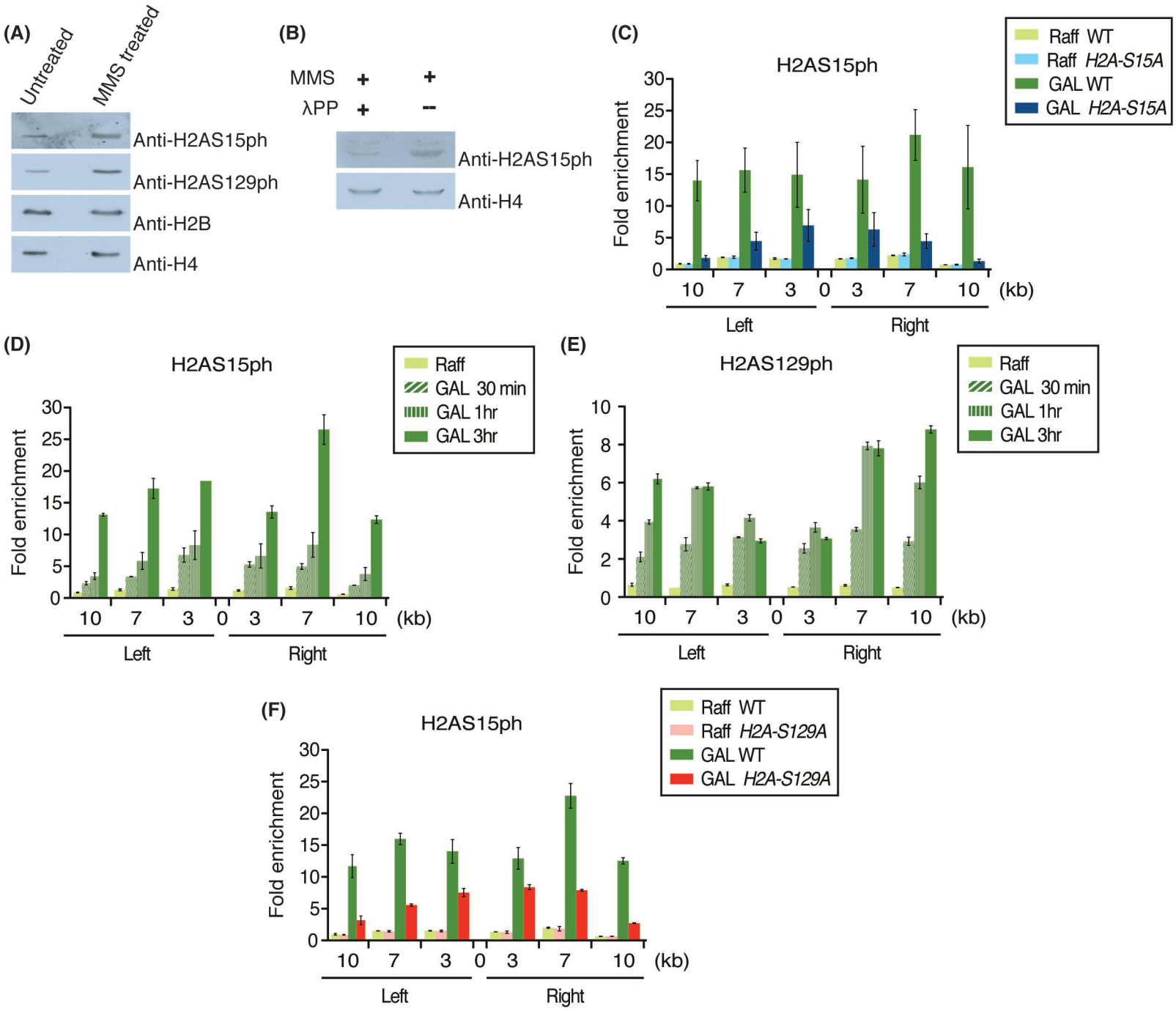
(A)
Untreated
MMS treated
Anti-H2AS15ph
Anti-H2AS129ph
Anti-H2B
Anti-H4
(B)
MMS + +
λPP + −
Anti-H2AS15ph
Anti-H4
(C)
H2AS15ph
Raff WT
Raff H2A-S15A
GAL WT
GAL H2A-S15A
Fold enrichment
0 5 10 15 20 25 30
10 7 3 0 3 7 10 (kb)
Left
Right
(D)
H2AS15ph
Raff
GAL 30 min
GAL 1hr
GAL 3hr
Fold enrichment
0 5 10 15 20 25 30
10 7 3 0 3 7 10 (kb)
Left
Right
(E)
H2AS129ph
Raff
GAL 30 min
GAL 1hr
GAL 3hr
Fold enrichment
0 2 4 6 8 10
10 7 3 0 3 7 10 (kb)
Left
Right
(F)
H2AS15ph
Raff WT
Raff H2A-S129A
GAL WT
GAL H2A-S129A
Fold enrichment
0 5 10 15 20 25 30
10 7 3 0 3 7 10 (kb)
Left
Right

FIGURE 3

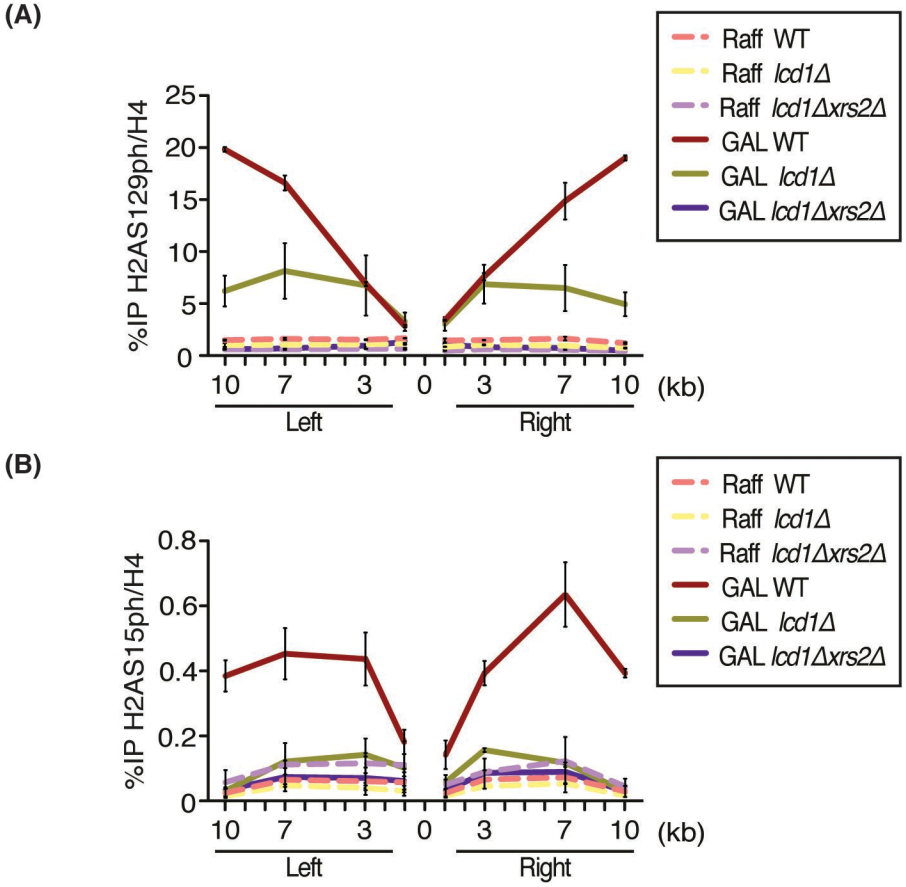
(A)
%IP H2AS129ph/H4
25
20
15
10
5
0
10 7 3 0 3 7 10 (kb)
Left
Right
Raff WT
Raff lcd1Δ
Raff lcd1Δxrs2Δ
GAL WT
GAL lcd1Δ
GAL lcd1Δxrs2Δ
(B)
%IP H2AS15ph/H4
0.8
0.6
0.4
0.2
0
10 7 3 0 3 7 10 (kb)
Left
Right
Raff WT
Raff lcd1Δ
Raff lcd1Δxrs2Δ
GAL WT
GAL lcd1Δ
GAL lcd1Δxrs2Δ

FIGURE 4

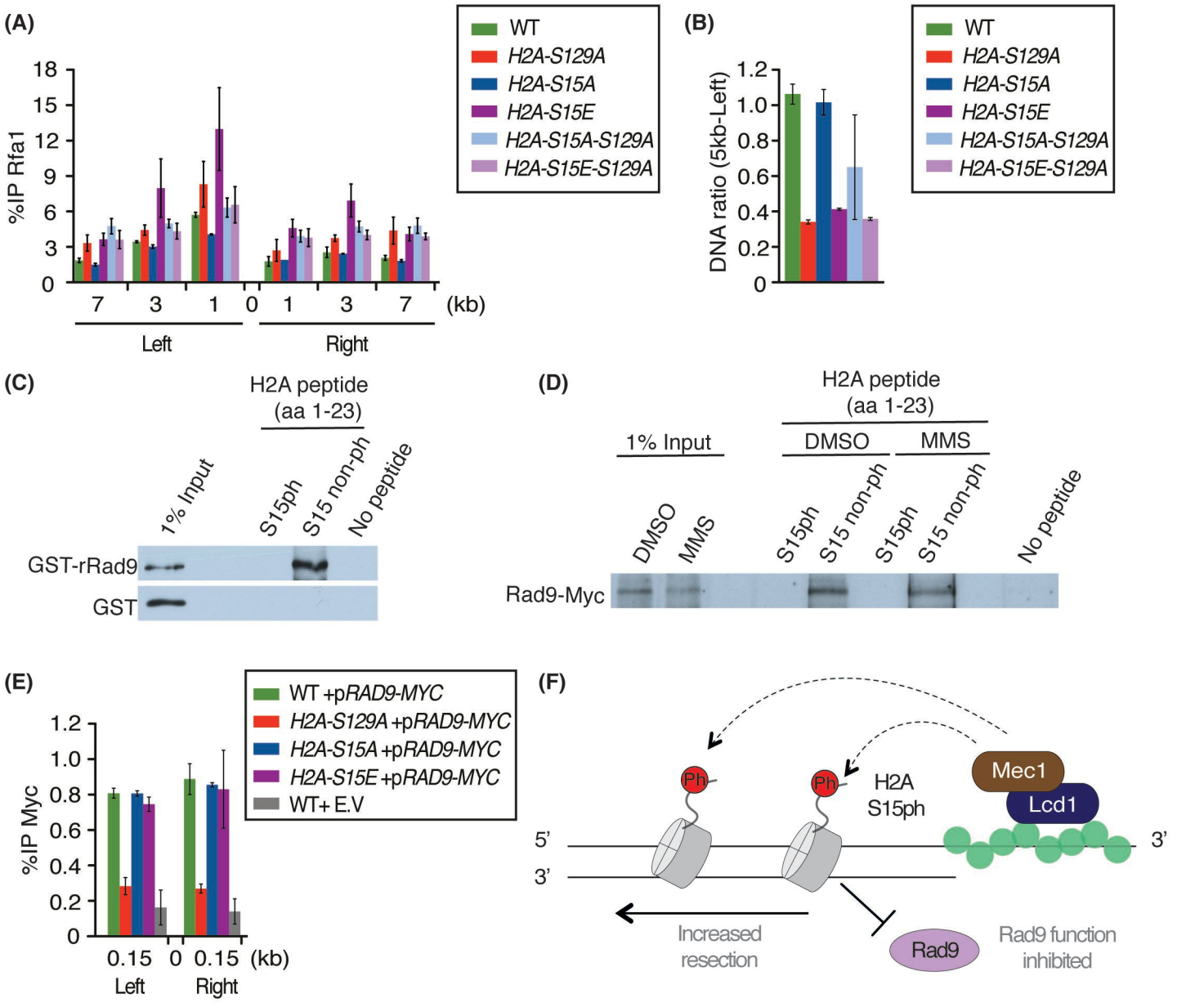
(A)
%IP Rfa1
18
15
12
9
6
3
0
7
3
1
0
1
3
7
(kb)
Left
Right
WT
H2A-S129A
H2A-S15A
H2A-S15E
H2A-S15A-S129A
H2A-S15E-S129A
(B)
DNA ratio (5kb-Left)
1.2
1.0
0.8
0.6
0.4
0.2
0
WT
H2A-S129A
H2A-S15A
H2A-S15E
H2A-S15A-S129A
H2A-S15E-S129A
(C)
H2A peptide
(aa 1-23)
1% Input
S15ph
S15 non-ph
No peptide
GST-rRad9
GST
(D)
H2A peptide
(aa 1-23)
1% Input
DMSO
MMS
DMSO
MMS
S15ph
S15 non-ph
S15ph
S15 non-ph
No peptide
Rad9-Myc
(E)
%IP Myc
1.2
1.0
0.8
0.6
0.4
0.2
0
0.15
0
0.15
(kb)
Left
Right
WT +pRAD9-MYC
H2A-S129A +pRAD9-MYC
H2A-S15A +pRAD9-MYC
H2A-S15E +pRAD9-MYC
WT+ E.V
(F)
Ph
Ph
H2A
S15ph
Mec1
Lcd1
5'
3'
3'
Increased
resection
Rad9
Rad9 function
inhibited